ELSEVIER

Composites Science and Technology 62 (2002) 1381–1395

COMPOSITES SCIENCE AND TECHNOLOGY

www.elsevier.com/locate/compscitech

A stochastic plasticity approach to strength modeling of strand-based wood composites

Peggi L. Clouston[a,*], Frank Lam[b]

[a]Department of Natural Resources Conservation, University of Massachusetts, 160 Holdsworth Way, Amherst, MA 01003- 9285, USA

[b]Department of Wood Science, University of British Columbia, FSC 4041- 2424 Main Mall, Vancouver, BC, Canada V6T 1Z4

Received 19 November 2001; received in revised form 26 April 2002; accepted 2 May 2002

Abstract

A 3 dimensional stochastic finite element technique is presented herein for simulating the nonlinear behaviour of strand-based wood composites with strands of varying grain-angle. The approach is based on the constitutive properties of the individual strands to study the effects of varying strand characteristics (such as species or geometry) on the performance of the member. The constitutive properties of the strands are found empirically and are subsequently used in a 3 dimensional finite element program. The program is formulated in a probabilistic manner using random variable material properties as input. The constitutive model incorporates classic plasticity theory whereby anisotropic hardening and eventual failure of the material is established by the Tsai–Wu criterion with an associated flow rule. Failure is marked by an upper bound surface whereupon either perfect plasticity (i.e. ductile behavior) or an abrupt loss of strength and stiffness (i.e. brittle behavior) ensues. The ability of this technique to reproduce experimental findings for the stress–strain curves of angle-ply laminates in tension, compression as well as 3 point bending is validated.
© 2002 Elsevier Science Ltd. All rights reserved.

Keywords: A. Wood; B. Modelling; B. Non-linear behaviour; C. Computational simulation; C. Failure criterion

1. Introduction

Structural composite lumber (SCL) is a relatively new division of structural building materials which are rapidly gaining recognition and acceptance in today's construction industry. The generic term, SCL, refers to products such as: laminated veneer lumber (LVL), parallel strand lumber (PSL), laminated strand lumber (LSL), and thick oriented strand board/rimboard. These new engineered wood products have more consistent mechanical and physical properties than conventional lumber owing to their sophisticated manufacturing processes whereby thin wood veneers, strands or flakes which are arranged and bonded together using adhesive under controlled heat and pressure. Due to this high consistency and consequential improved strength properties, structural composite lumber is replacing conventional lumber in traditional wood applications (i.e. beams and columns) and, moreover, are starting to be used in applications typically dominated by steel or concrete (i.e. long span commercial roof trusses and shell structures).

Numerical models can be powerful and effective tools for the accurate design and future development of structural composite lumber. However, due to the relative immaturity of these products in the market place, viable methods for modeling their fundamental mechanical behaviour have yet to be fully explored. Only a few studies to date have focused on computational modeling of wood-based composites. An early study by Hunt and Suddarth [1] used linear elastic finite element analysis together with the Monte Carlo technique to predict tensile and shear modulus of medium

* Corresponding author. Tel.: +1-413-545-1884; fax: +1-413-545-4358.

E-mail addresses: clouston@forwild.umass.edu (P.L. Clouston), franklam@interchange.ubc.ca (F. Lam).

0266-3538/02/$ - see front matter © 2002 Elsevier Science Ltd. All rights reserved.
PII: S0266-3538(02)00086-6

Nomenclature

[B]	strain-displacement matrix
F_{12}	strength tensor denoted the interaction parameter
M_{ij}	tensors of strength parameters
k	threshold stress
$\{P\}$	internal resisting force vector
S	in-plane shear strength
V	volume
X_t	longitudinal tensile strength
X_c	longitudinal compressive strength
Y_t	transverse tensile strength
Y_c	transverse compressive strength
α_i	parameters which define the offset of the yield surface
β	shape parameter of 2-parameter Weibull distribution
ρ_i	portion of effective stress
σ_I	stress components
τ	non-specific material strength

Subscripts
x, y, z = laminate coordinate directions; and 1, 2, 3 = principal material directions.

density homogeneous flakeboard. The model agreed well with the average experimental results with a maximum error of 13%. More recently, Triche and Hunt [2] developed a linear elastic finite element model capable of predicting the tensile strength and stiffness of a parallel aligned wood strand composite. The model considered each strand to have three layers (i.e. pure wood, resin and an interface) and the properties of the individual constituents were used as input. Excellent accuracy for the predicted modulus of elasticity was reported (from 0.0 to 11.1% error). However, prediction of maximum stress was inconsistent and in at least one case unacceptable (from 1.2 to 101.1% error). Cha and Pearson [3] developed a two dimensional finite element model to predict the elastic tensile properties of a 3 ply veneer laminate, consisting of an off-axis core ply of varying angles. Good agreement was obtained between predicted and experimental strains at maximum load (maximum difference of 14.3%) as well as predicted and experimental stresses (maximum difference of 7.7%). In 1998, Wang and Lam [4] developed a three dimensional nonlinear stochastic finite element model to estimate the probabilistic distribution of the tensile strength of parallel aligned wood strand composites based fundamentally upon longitudinal tensile strength and stiffness data of the individual strands. The model was verified through comparison of predicted and experimental data for four and six ply laminates. Most recently, Clouston and Lam [5] presented a two dimensional stochastic finite element approach for simulating the axial (tensile and compressive) stress–strain behavior of parallel aligned wood strand composites with strands of varying grain angle. The approach was based on nonlinear constitutive properties of the individual strands which were characterized within the framework of orthotropic elasto-plasticity. The constitutive model employed the Tsai–Wu yield criterion with an associated flow rule of plasticity. Predicted behaviour of $[\pm 15]_s$ and $[\pm 30]_s$ angle-ply laminates in tension and compression were shown to compare favorably with experimental results.

The present paper is an extension of the work by Clouston and Lam [5]. In this previous paper, simple planar elements were used under the assumption that interlaminar stresses associated with the through-thickness (z) direction were negligible. This assumption was appropriate for the configurations considered (i.e. symmetric laminates subjected to in-plane forces). The current model, in contrast, employs 3 dimensional brick elements in order that out-of-plane stresses can be examined. Consequently, the present formulation has the added capability to perform analyses on non-symmetric composite beams. This advancement is viewed as a necessary step towards the ultimate goal of predicting the constitutive behaviour of geometrically complex commercial wood composites, such as Parallam®, PSL.

The objective of this paper is to present the formulation and validation of a 3 dimensional finite element based model for simulating the constitutive behaviour of an academic wood composite with layers of varying fiber orientation as shown in Fig. 1. The finite element code is developed within a probabilistic framework using random variables as input enabling stochastic-based Monte Carlo simulation analyses.

2. Model development

2.1. Constitutive model

Orthotropic plasticity theory is utilized in describing the nonlinear behaviour up to and beyond the point of

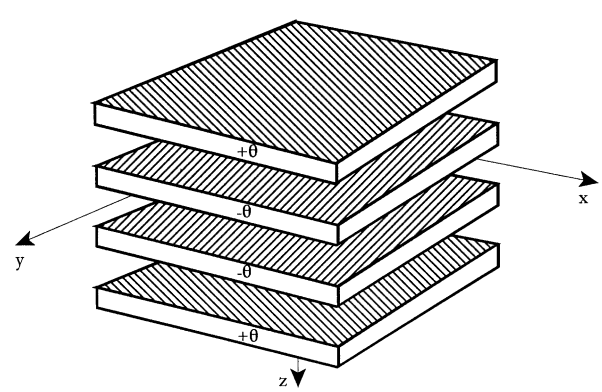

Fig. 1. Exploded view of a symmetric angle-ply laminate.

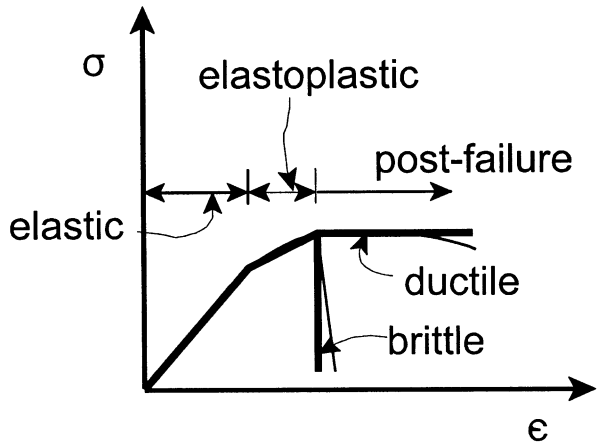

Fig. 2. Idealized constitutive behavior of material.

material failure. Referencing Fig. 2, the nonlinear constitutive behaviour of the wood strands is defined by four basic constitutive regimes: elastic, elasto-plastic, post-failure brittle, or post-failure ductile. Strain hardening is characterized by an associative flow rule where the yield surfaces are defined by a 2 dimensional (plane stress) form of the Tsai–Wu polynomial failure criterion [6]. A plastic formulation is adopted [7] whereby the initial and successive yield surfaces are defined in index notation as

$$f \equiv M_{ij}(\sigma_i - \alpha_i)(\sigma_j - \alpha_j) - k^2 = 0 \tag{1}$$

where: σ_i are applied stresses, $i, j = 1, 2, 6$ and M_{ij} are strength tensors defined as

$$M_{ij} = X_t X_c \begin{bmatrix} \frac{1}{X_t X_c} & F_{12} & 0 \\ F_{12} & \frac{1}{Y_t Y_c} & 0 \\ 0 & 0 & \frac{1}{S^2} \end{bmatrix} \tag{2}$$

α_i are tensors describing the origin of the yield surface found from simultaneous solution of the equations:

$$\frac{1}{X_t} - \frac{1}{X_c} = -2 \cdot \left(\frac{1}{X_t X_c} \cdot \alpha_1 + F_{12} \cdot \alpha_2 \right) \tag{3a}$$

$$\frac{1}{Y_t} - \frac{1}{Y_c} = -2 \cdot \left(F_{12} \cdot \alpha_1 + \frac{1}{Y_t Y_c} \cdot \alpha_2 \right) \tag{3b}$$

k^2 is the square of the threshold stress determined as:

$$k^2 = X_t X_c + M_{ij} \alpha_i \alpha_j \tag{4}$$

and finally, Eqs. (2)–(4) are written in terms of the strengths in the principal material directions: tension and compression parallel to grain (X_t and X_c), tension and compression perpendicular to grain (Y_t, Y_c), in-plane shear (S) and a normal stress interaction parameter (F_{12}).

The 2 dimensional form of the Tsai–Wu criterion was chosen instead of a 3 dimensional form for simplicity. A thorough investigation of parameters required for the 3 dimensional form was deemed to be, at this stage of modeling, overly time and cost prohibitive. Moreover, it was decided that since the cases being investigated could be considered to be under plane stress conditions, a plane stress criterion would suffice. In any case, as the 3 dimensional model produces estimates of the out-of-plane stresses, this assumption could be readily verified or subsequent changes made to the criterion, if necessary.

As shown in Fig. 2, upon initial detection of failure of an integration point, the material responds either in an elasto-plastic manner (for a compression dominant stress state) or a brittle manner (for a tension dominant stress state). The distinction is made depending on the combination of stresses at the point of failure. In order to define conditions for tension dominance, we first define variables which reflect the magnitude of the individual stress components as

$$\begin{aligned} \rho_1 &= M_{11}\left[\sigma_1^2 - 2\sigma_1\alpha_1 + \alpha_1^2\right] \\ \rho_2 &= M_{22}\left[\sigma_2^2 - 2\sigma_2\alpha_2 + \alpha_2^2\right] \\ \rho_4 &= M_{44} \cdot \sigma_4^2 \end{aligned} \tag{5}$$

The conditions for tension dominance for the 3 dimensional model are then (1) $\sigma_1 \geqslant X_t$; (2) $\sigma_2 \geqslant Y_t$; (3) $|\sigma_6| \geqslant S$; (4) $\sigma_1 \geqslant 0$ and $\rho_1 \geqslant \rho_2$; (5) $\sigma_2 \geqslant 0$ and $\rho_2 \geqslant \rho_1$; (6) $\rho_4 \geqslant \rho_1$ and $\rho_4 \geqslant \rho_2$; and (7) $\left|\frac{\sigma_4}{S}\right| \geqslant \left|\frac{\sigma_1^+}{X_t}\right|$ or $\left|\frac{\sigma_1^-}{X_c}\right|$. These conditions were established semi-empirically: chosen primarily based on known mechanical behaviour of wood but also chosen to provide a favorable comparison between simulated and experimental behaviour of control tests—$[\pm 15]_s$ angle-ply laminate under compression loading. These same experimental results were used to establish material input parameters (S, G and F_{12}) for the model as discussed in Section 2.4.

In the case of a tension dominant failure, the stress level is reduced gradually to facilitate convergence of the iterative procedure. Upon the first iteration of each load increment following brittle failure, the stresses at the failed integration point are reduced to 90, 90, 95 and 98% of the previous value, for σ_1 (when tensile), σ_2, σ_6, and σ_1 (when compressive), respectively. The loss in stress at the failed point is compensated for by an increase in the stress carried by adjacent Gaussian points. System equilibrium is attained through an iterative process as described in Section 2.3.

In the case of a compression dominant failure, the point initially undergoes strain hardening in accordance with a general anisotropic hardening model. The threshold stress (k) as well as the parallel and perpendi-

cular-to-grain compressive strengths (X_c and Y_c) vary with plastic deformation resulting in expansion while at the same time distortion of the yield surface. Upon ultimate failure, the final values of the compressive strengths remain constant emulating perfect plasticity.

2.2. Finite element formulation

The foregoing constitutive model was implemented into a, stochastic, materially nonlinear 3 dimensional finite element program. The program is based on the conventional displacement method using linear solid (8 node brick) isoparametric elements. For each element, a 2-point Gauss quadrature rule is used. The width of each element coincides with the thickness of each strand in order that strength and stiffness properties can easily vary according to strand. To avoid singularities in the structural stiffness matrix, the laminate was loaded by prescribing an increasing value of displacement while maintaining initial stiffness throughout the entire analysis. For each increment in displacement, the nonlinearities in the equilibrium equations were resolved using a modified Newton–Raphson iterative solution technique as described below.

2.3. Computational procedure

An abbreviated outline of the computational procedure used to simulate load-displacement behaviour of N wood laminates is as follows:

Arrays of random numbers are first generated for random strengths and stiffnesses in accordance with input file parameters. Then, for each of the N replications:

1. Laminate geometry and boundary conditions are read from an input file and used in a materially nonlinear finite element subprogram (to calculate a load displacement curve).
2. Element stiffnesses for elastic (or elastoplastic) behaviour are determined using random numbers for the given replication and the global stiffness matrix is assembled.
3. Principal material strength values (X_t, Y_t, X_c, Y_c, S and F_{12}) are generated based on the random numbers allotted for the replication.
4. Displacements are incremented according to a prescribed factor.
5. The system of simultaneous equations is solved.
6. Incremental nodal displacements and Gauss point strains are calculated.
7. Incremental stresses are computed (depending on stage of plasticity) and are transformed into the principal material directions. Stage of plasticity of each Gaussian point is determined through implementation of Eq. (1).
8. Total stresses are updated for each point. A vector of nodal forces $\{P\}$, which are statically equivalent to the stress field satisfying elastoplastic conditions, is calculated as

$$\{P\} = \int_V [B]^T \{\sigma\} \mathrm{d}V \tag{6}$$

where $[B]$ is the strain-displacement matrix and $\{\sigma\}$ is the vector of updated stresses for each point. This vector is calculated for comparison against the total force vector $\{F\}$ to establish system equilibrium as described in Owen and Hinton [8].

9. A residual force vector $\{\Psi\} = \{F\} - \{P\}$ is computed and checked against the convergence criteria:

$$\frac{\sqrt{\{\Psi\}^T\{\Psi\}}}{\{F\}^T\{F\}} \leqslant 0.01 \tag{7}$$

If convergence is not met, then the procedure iterates from step 5, where the global system of equations is solved based on the residual force vector $\{\Psi\}$. When convergence is met, another load increment is applied.

This incremental-iterative procedure continues until final failure which occurs when the load displacement curve begins to descend. The replication is considered finished and is automatically stopped when the load reaches 90% of the peak load. In rare cases, the replication may also be halted due to non-convergence beyond peak load. The 90% condition was chosen in consideration of both computer time and numerical instability.

2.4. Program input

The mechanical properties of the strands, which are required program inputs, were established using Coastal Douglas-fir strands through both experimental and analytical techniques. The properties associated with X_c, Y_c, X_t, and Y_t were acquired through simple uniaxial tests.

Tensile tests were conducted at the University of British Columbia using a servo-hydraulic 250 kN Material Testing System (MTS) machine under deflection control mode. Mechanical wedge- action grips were used and a 25.4 mm gauge length extensometer was employed to establish tensile stiffness. For tension parallel-to-grain properties, individual strands (3 mm×19 mm×50 mm) were used. For tension perpendicular-to-grain properties, however, small laminates (17 mm×19 mm×152 mm^3) consisting of 6 strands each were used to avoid breakage during handling.

Compression tests were conducted at the Laboratoire de Mechanique et Technologie (LMT), École Normale Supérieure (ENS), Cachan-University Paris, France.

Table 1
Results of nonlinear minimization

Statistics (1)	$[\pm 15]_s$ Compression		S (4)	G (5)	F_{12} (6)
	Experiment (2)	Simulation (3)			
Avg. (MPa)	51.57	51.28	11.4	392.2	1.067×10^{-03} MPa^{-2}
COV (%)	14.42	51.28	21.8	21.7	8.78

Table 2
Input properties for $[\pm 15]_s$ and $[\pm 30]_s$ angle ply laminates (compression, shear and F_{12})

	Property (1)	Mean (2)	S.D. (3)
Parallel-to-grain compression	Elastic modulus (MPa)	10090	1930
	Yield strength (X_c) (MPa)	67.3	13
	Tangent modulus (MPa)	1926	639
	Ultimate strength ($X_c{}^u$) (MPa)	76.5	5.4
Perpendicular-to-grain compression	Elastic modulus (MPa)	490	74.6
	Yield strength (Y_c) (MPa)	15.4	1.8
	Tangent modulus (MPa)	110	38.6
	Ultimate strength ($Y_c{}^u$) (MPa)	18.2	1.7
In-plane shear	Shear modulus (G) (MPa)	392.2	85.1
	Strength (S) (MPa)	11.4	2.6
Interaction parameter	F_{12} (MPa^{-2})	1.1×10^{-03}	9.4×10^{-05}

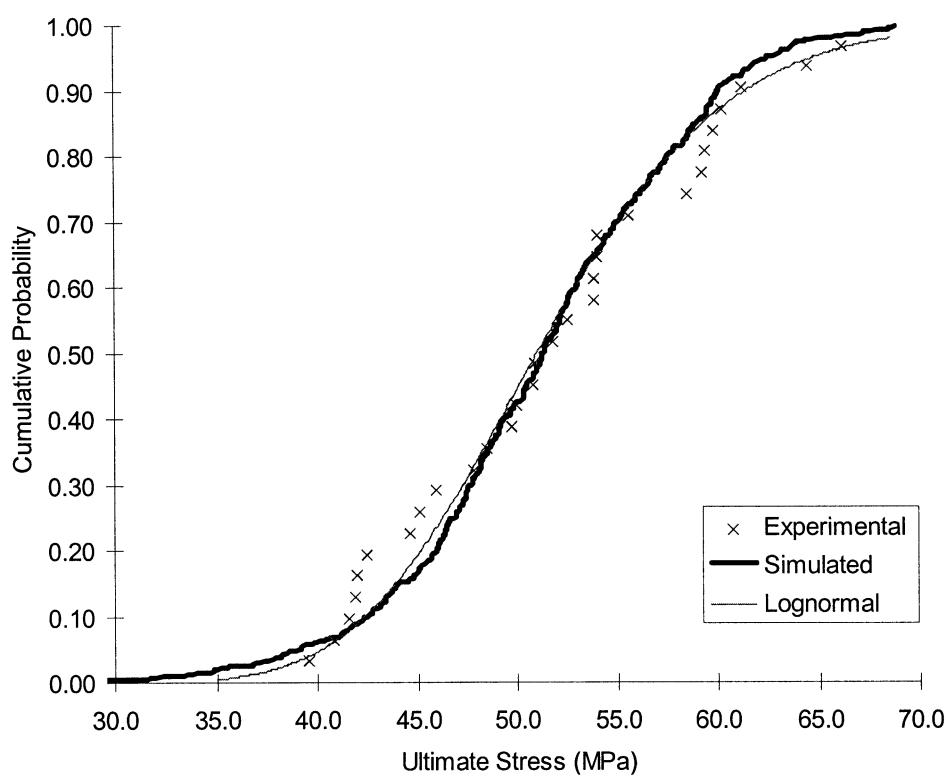

Fig. 3. Cumulative probability distribution of $[\pm 15]_s$ laminate in compression (fitted results).

Tests were performed using a 50 kN MTS machine equipped with a linear variable displacement transducer (LVDT) to measure cross head displacement. Swivel bearings, both top and bottom, were used to prevent eccentric loading on the specimen. Compression tests were performed on 6-ply laminated specimens (17 mm×19 mm×50 mm) to satisfy short column requirements and thereby avoid bucking.

Properties for shear and the interaction parameter, F_{12} (reference Table 1) were estimated through a non-

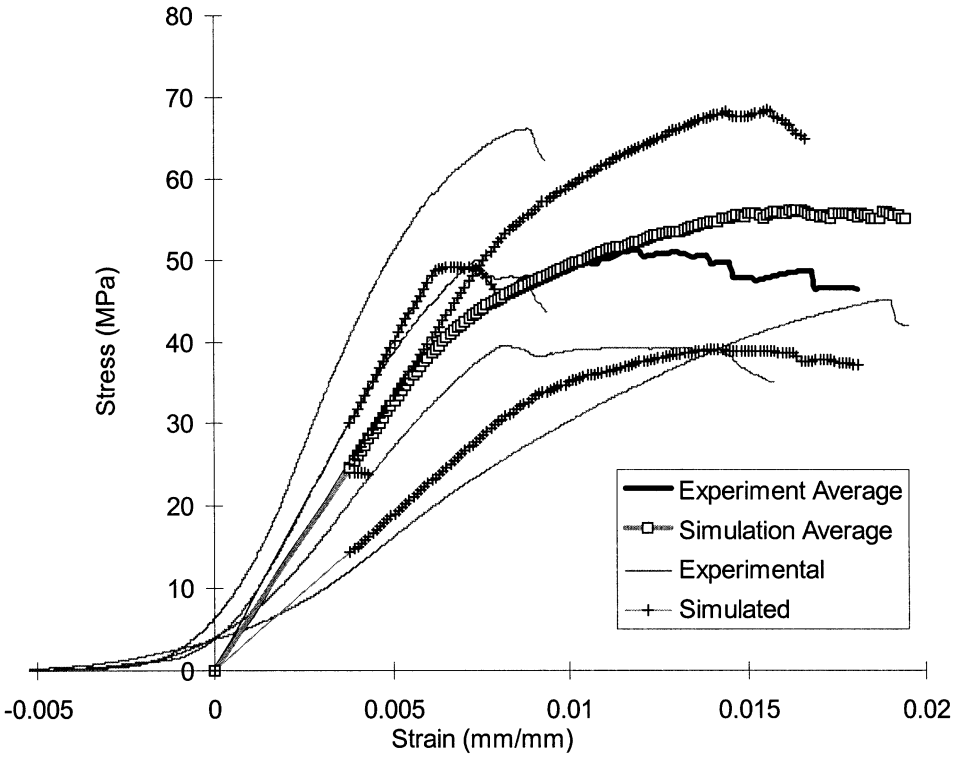

Fig. 4. Stress–strain curves of $[\pm 15]_s$ angle-ply laminate in compression.

linear least square minimization of error between predicted and experimental compression strengths of a $[\pm 15]_s$ angle-ply laminate. The procedure was described in detail in Clouston [5] and will not be repeated here. A visual depiction of the fitted data (500 points) versus the experimental data (31 points), as well as a log–normal curve for reference is given in Fig. 3. The predicted average and variability are very accurate, as expected.

The program is also adept at reproducing the stress–strain curves for this configuration. Fig. 4 illustrates a comparison of the simulated and predicted curves. For clarity, 5 curves for each data set are shown which represent the average as well as the upper and lower bound of both stiffness and strength. The average curves were obtained by sequentially averaging stress along constant lines of strain. It is noted that the average curves serve only as a reference and are not indicative of material response, per se; particularly within the higher strain range where the average values are based on fewer points because of varying total strain range.

Referencing Table 2, the average values and variability obtained for S, G and F_{12} are reasonable when compared to published data. It is important to note that these values in essence, serve to calibrate the model and are expected to produce different results for different models. For example, although within the same range, these values differ from those obtained from the 2 dimensional model.

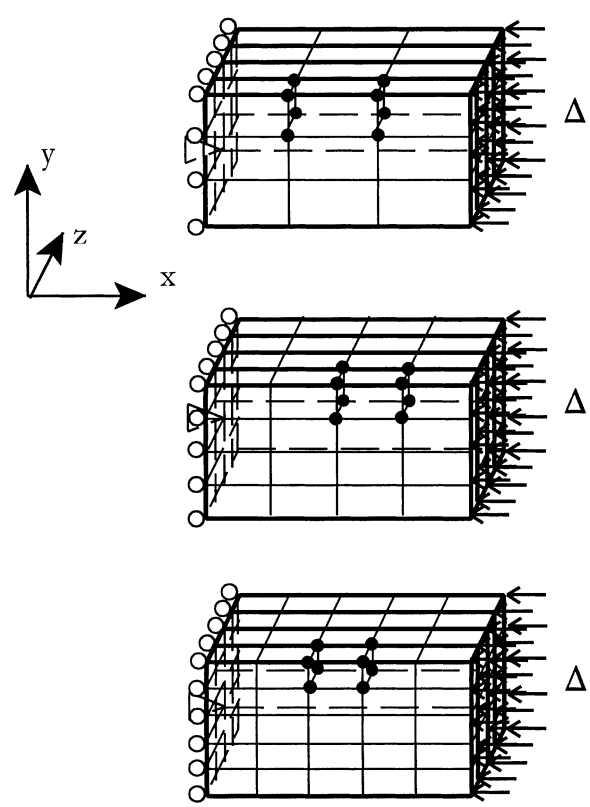

Fig. 5. Various mesh grades investigated: (a) 3×3 grid, (b) 4×4 grid, (c) 5×5 grid.

3. Numerical predictions

After having obtained all necessary mechanical properties, the program was utilized to predict the load-displacement behaviour of coastal Douglas-fir strand-based laminates up to and beyond failure. Five test configurations were investigated to verify the ability of the model to reproduce experimental findings: $[\pm 15]_s$ laminates in tension and 3 point bending as well as $[\pm 30]_s$ laminates in tension, compression and 3 point bending.

3.1. Mesh convergence study

A study was carried out to establish a cost efficient yet numerically accurate finite element mesh for the analyses. Three mesh sizes using simple rectangular elements were

Table 3
Input properties for mesh convergence study

	Property (1)	Mean (2)	S.D. (3)
Parallel-to-grain tension	Elastic modulus (E_Xt) (MPa)	15463	0
	Strength (X_t) (MPa)	72.8	0
Perpendicular-to-grain tension	Elastic modulus (E_{Yt}) (MPa)	91.2	0
	Strength (Y_t) (MPa)	6.5	0
Parallel-to-grain compression	Elastic modulus (E_{Xc}) (MPa)	10090	0
	Yield strength (X_c) (MPa)	67.3	0
	Tangent modulus (E_{Xc}') (MPa)	1926	0
	Ultimate strength ($X_c{}^u$) (MPa)	76.5	0
Perpendicular-to-grain compression	Elastic modulus (E_{Yc}) (MPa)	490	0
	Yield strength (Y_c) (MPa)	15.4	0
	Tangent modulus (E_{Yc}') (MPa)	110	0
	Ultimate strength ($Y_c{}^u$) (MPa)	18.2	0
Interaction parameter	F_{12}	1.067×10^{-03}	0
In plane shear	Elastic modulus (G) (MPa)	392.2	0
	Strength (S) (MPa)	11.4	0
Poisson's ratio	ν_{12}	0.32	–

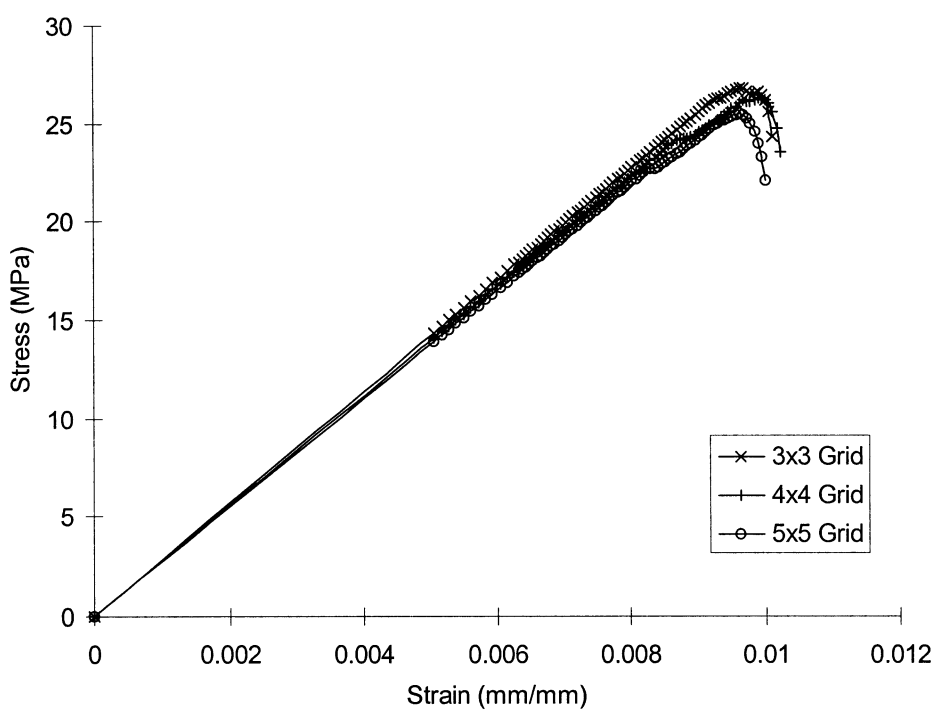

Fig. 6. Stress–strain diagrams of 3 investigated grids.

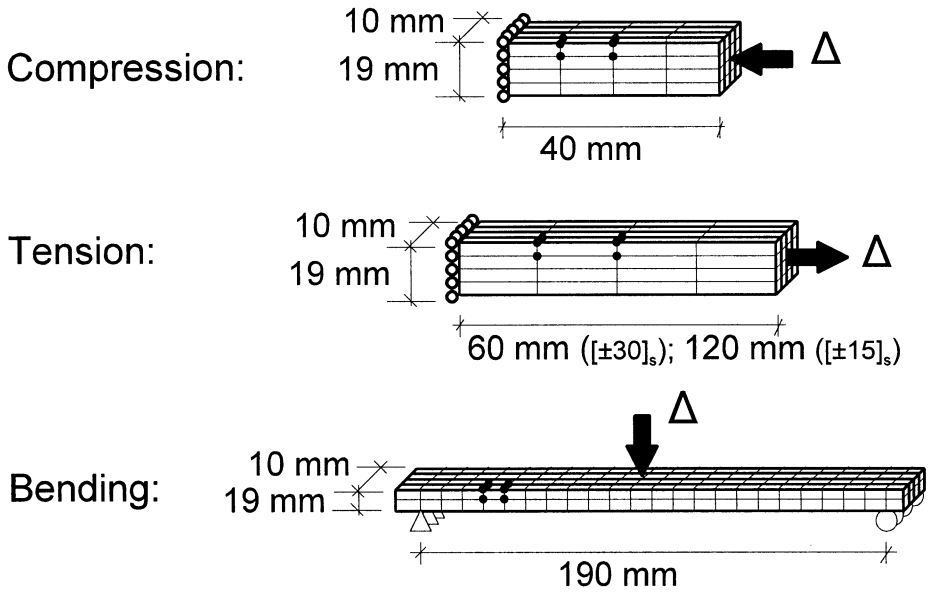

Fig. 7. Finite element mesh for each load configuration.

Table 4
Input tensile properties for $[\pm 15]_s$ and $[\pm 30]_s$ angle ply laminates

	Property (1)	Compression		Tension		Bending	
		Mean (2)	S.D. (3)	Mean (4)	S.D. (5)	Mean (6)	S.D. (7)
Parallel-to-grain tension	Elastic modulus (MPa)	15463	4716.2	15463	4716.2	15463	4716.2
	Strength (X_t) $[\pm 15]_s$ (MPa)	72.8	19.4	56.1	14.9	134.4	35.8
	Strength (X_t) $[\pm 30]_s$ (MPa)	72.8	19.4	66.1	17.6	136.2	36.3
Perpendicular-to-grain tension	Elastic modulus (MPa)	91.2	22.3	91.2	22.3	91.2	22.3
	Strength (Y_t) $[\pm 15]_s$ (MPa)	6.5	1.1	5.5	0.96	5.8	1.1
	Strength (Y_t) $[\pm 30]_s$ (MPa)	6.5	1.1	6.1	1.07	5.9	1.1

Table 5
Experimental and simulated data for $[\pm 30]_s$ angle ply laminates in compression

Statistic (1)	Experiment (2)	Simulation (3)	Error (%) (4)
Elastic modulus mean (MPa)	3052	2742	10.2
Elastic modulus COV (%)	27.5	8.3	69.8
Ultimate strength mean (MPa)	20.3	21.1	3.8
Ultimate strength COV (%)	11.1	13.8	23.9

investigated. In one case, a rather coarse mesh was used dividing the x and y dimensions into thirds (3×3 grid). The second was refined to a 4×4 grid and the third was refined further to a 5×5 grid. All three are illustrated in Fig. 5.

A $[\pm 30]_s$, angle-ply laminate subjected to compressive displacement was modeled. To ensure comparability between meshes, a deterministic analysis was performed. The same strength and stiffness variables, outlined in Table 3, were used for each case. The results of the three analyses are given graphically in Fig. 6.

The ultimate load for each case varies slightly with progressively lower predictions for the finer grids (26.8, 26.3 and 25.5 MPa for the coarse, average and fine mesh, respectively). This was a result of stress concentrations at the boundaries. The smaller elements produced higher stresses for equal displacement and thus failed earlier. Considering the results were relatively consistent, it was decided that the best element for both efficiency and accuracy would be the 4×4 grid.

The geometrical properties, finite element mesh and boundary conditions for each load configuration are given in Fig. 7. The mesh for the tensile and compressive loading contains 64 elements and 125 nodes and for bending, 176 elements and 345 nodes. The statistical parameters of the elastic and strength properties used

for input into the program are summarized in Tables 2 and 4. The tensile properties are regarded separately in Table 4 due to the manner of handling size effect.

3.2. Size effect adjustment

Prior to implementing experimental tensile values into finite element code, adjustments must first be made for size effect. Size effect is a widely known and generally accepted phenomenon particularly for wood, whereby large members, having a higher probability of containing a larger flaw (or weaker zone) than smaller members, result in lower strength [9–11]. For the tension and compression analyses in the present paper, the familiar relationship:

$$\frac{\tau_1}{\tau_2} = \left(\frac{V_2}{V_1}\right)^{\frac{1}{\beta}} \tag{8}$$

was used to make strength adjustments, where the strengths τ_1 and τ_2 correspond to the volumes V_1 and V_2, respectively and β is the shape parameter of the 2-parameter Weibull distribution for that test configuration [12]. The perpendicular-to-grain tension strengths were assumed to vary between each integration point and were thus adjusted from representing that of the tested volume to that of the tributary area surrounding one Gaussian point. Longitudinal strength, on the other hand, was assumed to vary between strands and was thus adjusted from the experimental gauge length to the model gauge length. A sample calculation is provided below.

Considering the tension parallel-to-grain strengths for the tension analysis, strength was adjusted from the length of the experimental test strand (L_1) to the length of one strand in the prediction specimen (L_2) (assuming cross sections for both strands to be equal) as follows:

Given: $\beta = 4.23$ (calculated from a maximum likelihood approach); $X_{t1} = 68.77$ MPa (experimental mean value); $L_1 = 50.8$ mm; L_2 ($[\pm 15]_s$ laminate) = 120 mm; L_2 ($[\pm 30]_s$ laminate) = 60 mm then for the $[\pm 15]_s$ laminate

$$X_{t2} = X_{t1}\left(\frac{L_1}{L_2}\right)^{\frac{1}{\beta}} = 68.77\left(\frac{50.8}{120.0}\right)^{\frac{1}{4.23}} = 56.1 \text{ MPa}$$

and for the $[\pm 30]_s$ laminate

$$X_{t2} = X_{t1}\left(\frac{L_1}{L_2}\right)^{\frac{1}{\beta}} = 68.77\left(\frac{50.8}{60.0}\right)^{\frac{1}{4.23}} = 66.1 \text{ MPa.}$$

The coefficient of variation is assumed to remain the same as that found in the experiment.

For the bending analysis, the tension perpendicular-to-grain values, varying with each Gaussian point, were adjusted using Eq. (8). In so doing, it was assumed that stresses were uniformly distributed about each Gaussian point. The tension parallel-to-grain strength values were, on the other hand, adjusted for each strand. To do this, a load configuration effect was implemented.

3.3. Load configuration effect adjustment

Based on similar principles as for size effect, load configuration effect is a consequence of brittle material strength being dependant on the proportion of material that is highly stressed. For example, a pure tensile member, which has its entire volume highly stressed, has a higher probability of occurrence of a critical flaw and hence a lower strength than does a bending member of the same size which has less of its volume highly stressed. The relationship between tensile and bending failure stress is found to be [13]:

$$\frac{\sigma_{\max(t)}}{\sigma_{\max(b)}} = \left(\frac{V_b}{2V_t(\beta+1)^2}\right)^{\frac{1}{\beta}} \tag{9}$$

The tension parallel-to-grain strength for the 15° laminate (for example) is then adjusted as follows:

Given: $\beta = 4.2$ $X_{t1} = \sigma_{\max(t)} = 68.77$ MPa; $V_t = 18.8 \times 3.2 \times 50.3 = 3026.0$; mm^3; V_b (15° laminate) = $11.0/4 \times 190 \times 19 = 9927.5$ mm^3 then

$$X_{t2} = X_{t1} \cdot \frac{1}{\left(\frac{V_b}{2V_t(\beta+1)^2}\right)^{\frac{1}{\beta}}} = 68.8 \times \frac{1}{\left(\frac{9927.5}{2 \cdot 3026(4.2+1)^2}\right)^{0.24}} = 134.4 \text{ MPa}$$

It is noted that Eq. (9) is valid for the current laminate under consideration (ie. with a depth equal to that of one strand—19 mm). If laminates with several strands through the depth were considered, the formulation would need to be reassessed.

3.4. Out-of-plane elastic parameters

The elastic moduli associated with the through-thickness direction, E_3, G_{13} and G_{23}, have been estimated through general moduli relationships [14] as

$E_3 : E_2 \approx 1.6 : 1$

$G_{13} : G_{12} : G_{23} \approx 10 : 9.4 : 1$

The major Poisson's ratios in the out-of-plane dimension are estimated by approximate relationships for Douglas-fir [14]:

$\nu_{12} = 0.32$

$\nu_{13}/E_1 = 2.6 \times 10^{-05}$ MPa

$\nu_{23}/E_2 = 4.9 \times 10^{-04}$ MPa

and the reciprocal relationships

$$\frac{\upsilon_{ij}}{E_i} = \frac{\upsilon_{ji}}{E_j} \quad i, j = 1, 2, 3 \tag{10}$$

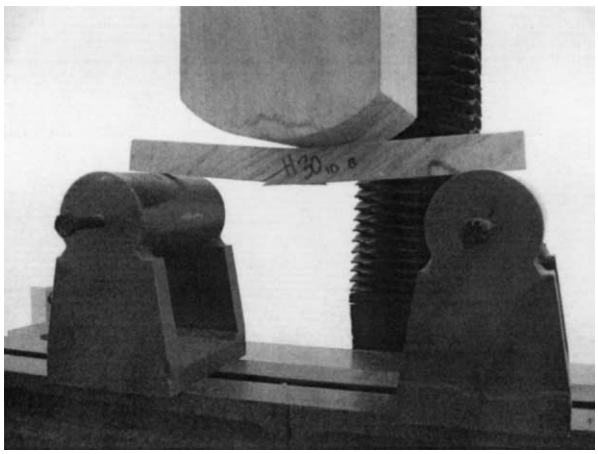

Fig. 8. Typical bending test set-up.

are invoked for the reciprocal identities. These elastic moduli are 100% correlated with the generated random value; for example, for each random value chosen for E_2, a new value for E_3 is calculated based solely on the given ratio.

4. Results

4.1. Experimental

For comparison to the numerical predictions, specimens were fabricated, conditioned and tested as follows.

4.1.1. Specimen preparation

Douglas-fir heartwood veneers were used in the fabrication of all specimens. The veneers were bonded together using PF 355H—a phenol-formaldehyde resin used in making commercial wood composites. The

Table 6
Experimental and simulated data for $[\pm 15]_s$ and $[\pm 30]_s$ angle ply laminates in tension

Configuration (1)	Statistic (2)	Experiment (3)	Simulation (4)	Error (%) (5)
$[\pm 15]_s$	Elastic modulus mean (MPa)	–	9128.6	–
	Elastic modulus COV (%)	–	12.8	–
	Strength mean (MPa)	39.4	36.4	7.6
	Strength COV (%)	16.7	17.5	4.8
$[\pm 30]_s$	Elastic modulus mean (MPa)	–	3132.7	–
	Elastic modulus COV (%)	–	10.85	–
	Strength mean (MPa)	21.7	21.4	1.4
	Strength COV (%)	9.0	13.2	46.7

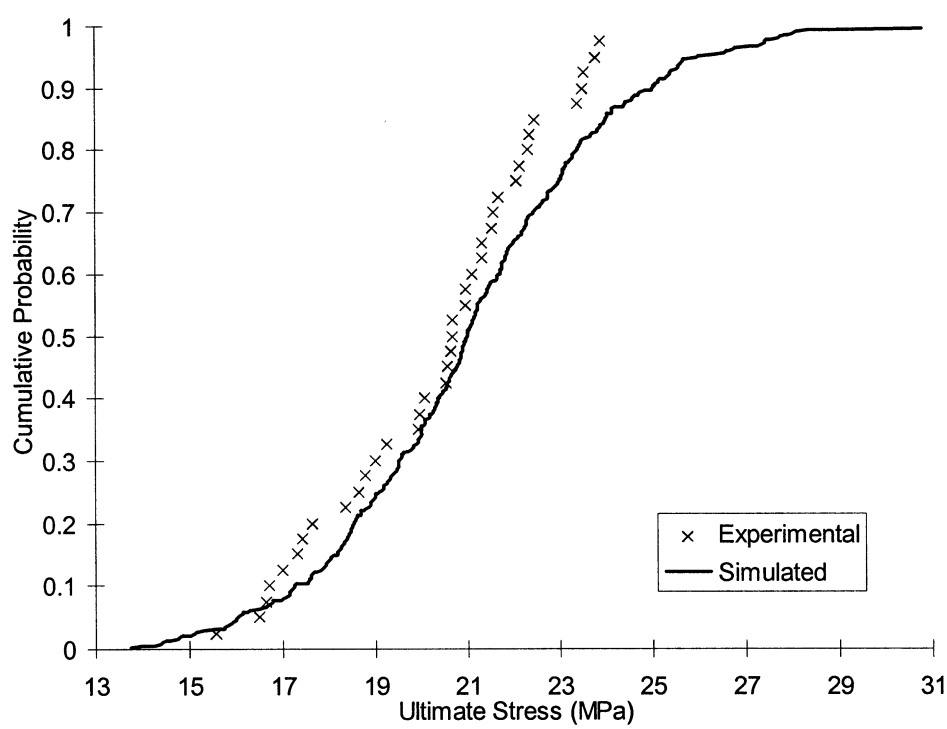

Fig. 9. Cumulative probability distribution of $[\pm 30]_s$ laminate in compression.

specimens were laminated and pressed using a 1600 kN capacity Pathex 760×760 mm^2 hot-press at 150 °C and 1.38 MPa pressure for 6 min.

All laminates were nominally 19×10.5 mm^2 in cross section and conditioned to approximately 7% moisture content. The compression specimens were cut to nominally 40 mm in length to comply with the requirements of ASTM D198–99 [15] for short columns with no lateral support. The $[\pm 15]_s$ tensile specimens were 120 mm in length and the $[\pm 30]_s$ laminates 60 mm in length. A longer test length was used for $[\pm 15]_s$ laminates to ensure wood fibres were not continuous from one test grip to the other, potentially increasing observed strength. Bending specimens were 190 mm in length.

4.1.2. Tests

Compression and 3 point bending tests were performed using a 133 kN capacity Sintech model 30/D universal testing machine. Load was applied under displacement control mode at a constant rate of 1.02 mm/min. A typical bending set-up is illustrated in Fig. 8. Tension tests were conducted using a 250 kN MTS universal test machine equipped with MTS mechanical wedge action grips. The loading rate was set at 1.8 mm/min to produce failure in 6 min, on average. Dimensions were measured at

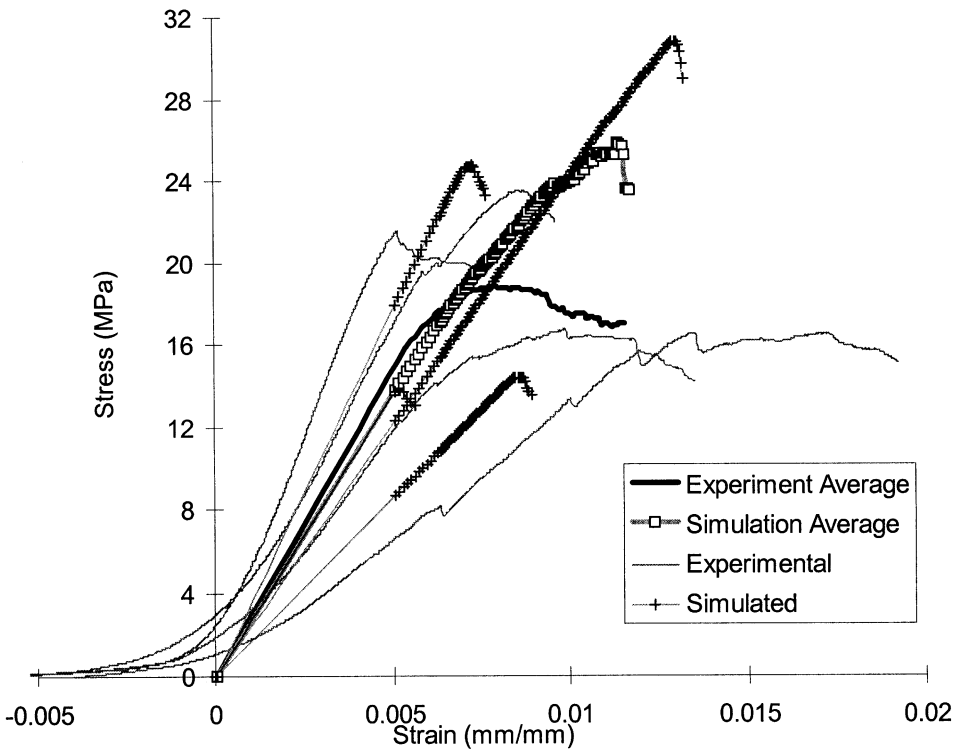

Fig. 10. Stress–strain curves of $[\pm 30]_s$ angle-ply laminate in compression.

Table 7
Experimental and simulated data for $[\pm 15]_s$ and $[\pm 30]_s$ laminates in 3 point bending

Configuration (1)	Statistic (2)	Experiment (3)	Simulation (4)	Error (%) (5)
$[\pm 15]_s$	Initial stiffness mean (MPa)	9023.3	8473.0	6.1
	Initial stiffness COV (%)	17.2	12.0	30.2
	Ultimate load mean (N)	825.6	849.8	2.9
	Ultimate load COV (%)	16.0	11.5	28.1
$[\pm 30]_s$	Initial stiffness mean (MPa)	4292.2	4925.9	14.8
	Initial stiffness COV (%)	5.7	11.6	103.5
	Ultimate load mean (N)	444.8	401.4	9.8
	Ultimate load COV (%)	8.9	8.7	2.2

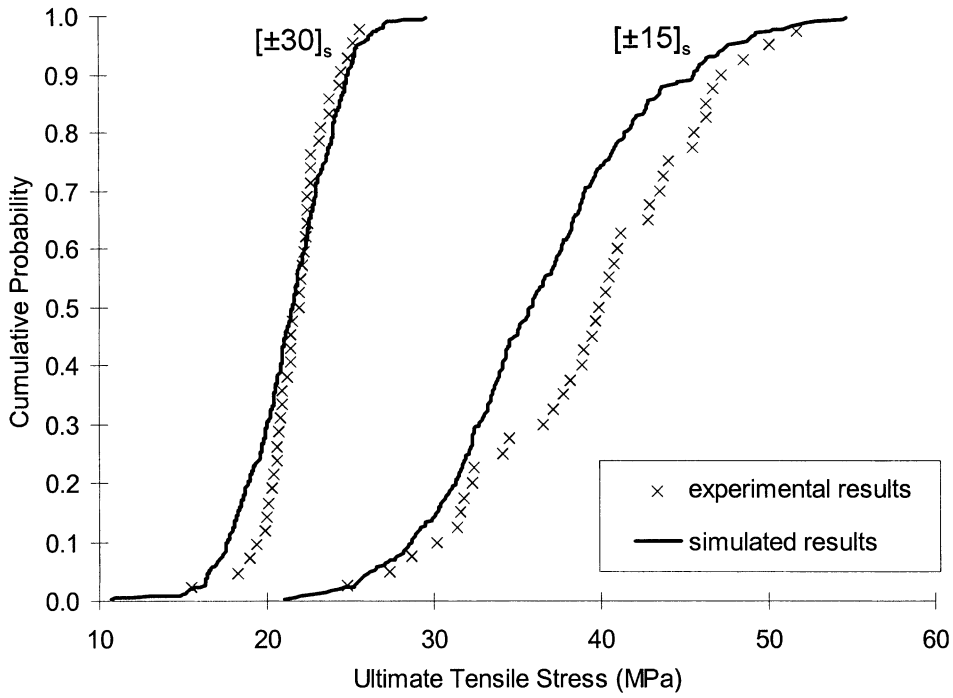

Fig. 11. Cumulative probability of $[\pm 15]_s$ and $[\pm 30]_s$ laminate in tension.

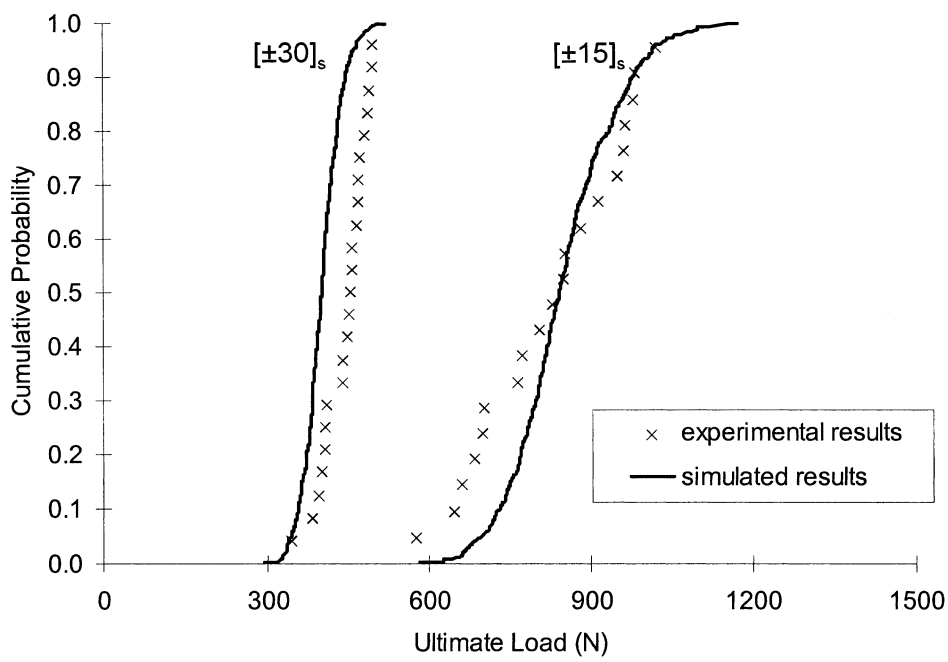

Fig. 12. Cumulative probability of $[\pm 15]_s$ and $[\pm 30]_s$ laminates in 3 point bending.

ends and mid-span using digital calipers and were found to be reasonably consistent with a maximum coefficient of variation of 1.8% for thickness and 0.4% for depth.

4.2. Comparison of experimental and simulated data

4.2.1. Compression results

The simulated and experimental results for the $[\pm 30]_s$ laminates are compared numerically in Table 5. The mean values for the elastic modulus and the ultimate strength are well predicted (10.2 and 3.8% error, respectively). This agreement is also illustrated graphically in Figs. 9 and 10. The cumulative probability distribution of the simulated results (500 replications) compares relatively well with that of the experimental results (39 tests) given a slightly high variability. The stress–strain curves in Fig. 10 demonstrate the program's ability to capture mode of failure. In this

configuration, failure is governed by in-plane shear and tension perpendicular-to-grain, which is modeled as being brittle. The point of failure on the curves (both experimental and simulated) is significantly more abrupt (brittle) than say, for that of the $[\pm 15]_s$ laminates shown in Fig. 4, where compression parallel-to-grain is more dominant. One can see from Fig. 10 that the stiffness of the simulated curves is less variable than the

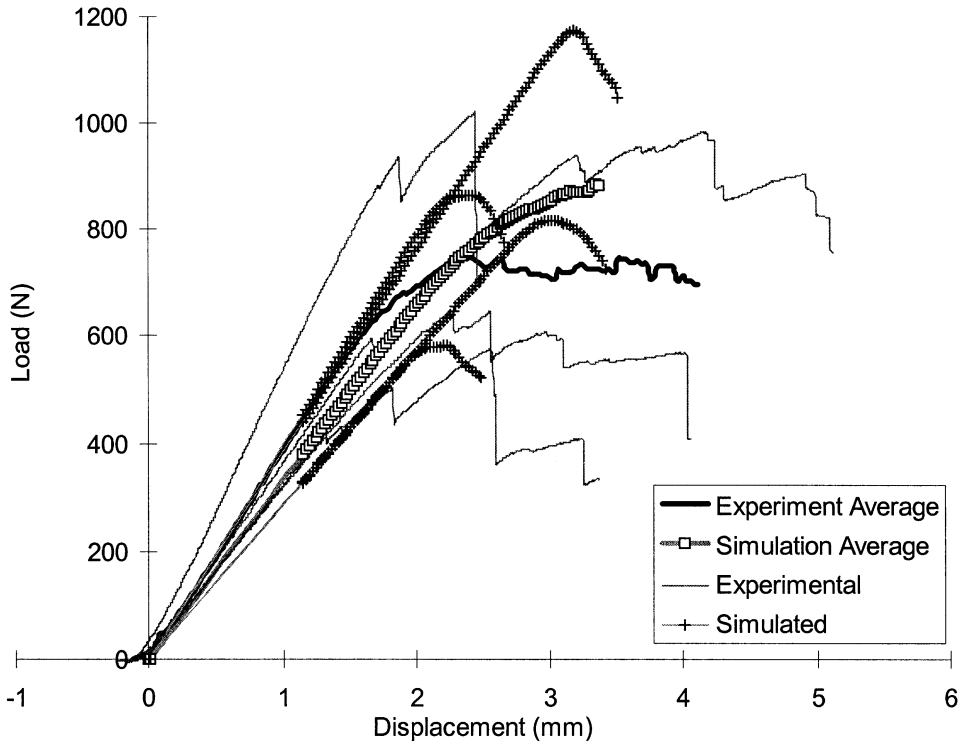

Fig. 13. Load-displacement curves of $[\pm 15]_s$ angle-ply laminate in 3 point bending.

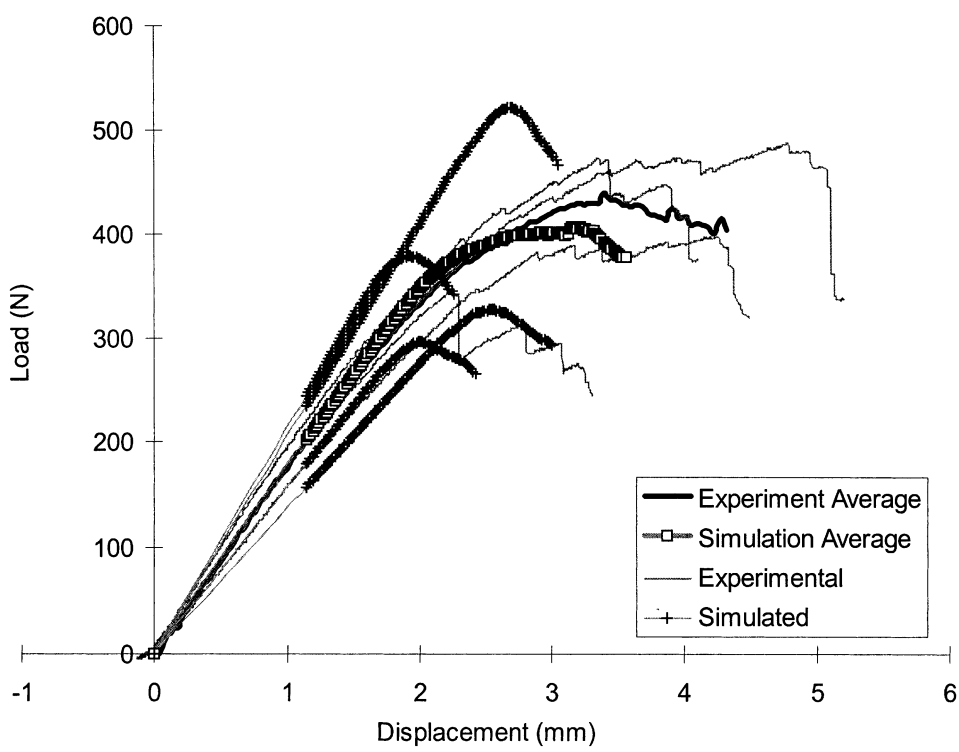

Fig. 14. Load-displacement curves of $[\pm 30]_s$ angle-ply laminate in 3 point bending.

experimental but clearly lay within the experimental bounds.

4.2.2. Tension results

Experimental and simulated tensile results are summarized in Table 6 and Fig. 11. The tension grips were of a wedge type such that as the load increased, the measured displacement of the specimen included inherent displacement within the grips. As a result, the stress–strain curves exhibit, incorrectly, a lower stiffness and thus cannot be compared to the simulated data. Regardless, descriptive statistics are included for the simulated elastic stiffness for completeness.

Ultimate strength is predicted relatively well for both configurations (maximum error of 7.6%). The coefficient of variation for strength is somewhat high, however, for the $[\pm 30]_s$ laminates. It is speculated that this occurs as a result of the variability for the fitted parameters, S (in-plane shear). This parameter was established using the $[\pm 15]_s$ laminate in compression, which is subject to a relatively low in-plane shear stress. Whereas, for the $[\pm 30]_s$ laminate in tension, shear stress governs. Inevitably, if the shear variability is estimated as being high, the $[\pm 30]_s$ tensile laminate variability will be high.

4.2.3. Bending results

Descriptive statistics for the 3 point bending results are outlined in Table 7 and cumulative probability distributions are plotted in Fig. 12. The mean value of the ultimate load as well as variability is relatively well predicted with a maximum error of 9.8 and 28.1%, respectively.

Figs. 13 and 14 illustrate the program's ability to replicate the load-displacement curves for the entire range of experimental and simulated results. The ductile behaviour of the laminates is apparent, as is the onset of ultimate failure by abrupt brittle behaviour. The program in its present state, however, is unable to capture the experimental feature of recovery where, upon abrupt local failure, the stresses redistribute to surpass the previous peak. This is likely a consequence of the slow release of stresses upon brittle failure to assure convergence of the system. The stresses do in fact redistribute numerically, but in a more gradual manner.

5. Discussion and conclusion

A continuum mechanics approach to simulate the mechanical behaviour of wood strand composites has been described in this paper. An orthotropic elastic–plastic-failure constitutive model was implemented into a 3 dimensional finite element based program. The nonlinear formulation was managed using classic orthotropic incremental plasticity theory. Stiffness and strength properties of the material were input as random variables and treated stochastically. This allowed for many replications of one configuration through Monte Carlo simulations to generate entire sample comparisons.

The effectiveness of the program to replicate experimental findings was demonstrated. The results of numerical simulations for angle-ply laminates in tension, compression and 3 point bending compared favorably with experimental data. These positive results indicate that the approach proposed herein offers an elegant solution to predicting wood composite behaviour. Indeed, the technique is general enough to be used for a variety of laminated composites provided the experimental database for the layer component of the composite is available. It is noted, however, that further research is required prior to being able to use the method for commercial products such as Parallam®, PSL.

For the plane stress conditions of this study, with symmetric laminates, a 2 dimensional form of the Tsai–Wu criterion proved adequate. That is to say, all analyses produced negligible out-of-plane stresses when compared to in-plane stresses. This is not necessarily the case when considering commercial wood composites due to their complex physical structure. These products typically have complicated, 3 dimensional staggered stacking sequences with overlapped and interwoven plys. For these products, a 3 dimensional stress state is highly likely and may warrant a 3 dimensional failure criterion.

An obvious improvement at this stage is to upgrade the program's ability to incorporate these physical characteristics. Several studies have been devoted to understanding and modeling the spatial relationships between individual wood elements in wood composites [16–19]. To incorporate these techniques into the present formulation may prove to be a difficult, although rewarding, task. It should entail consideration of density variations, potential null volumes or voids as well as varying 3 dimensional geometry of elements.

Acknowledgements

Gratitude is extended to Trus Joist Macmillan Ltd., Weyerhauser Ltd. and NSERC Canada (FSP 0166869) for providing funding for the project. As well, L'Ecole Normale Supérieure (ENS)-Laboratoire de Mécanique et Technologie-Cachan, France are acknowledged for providing facilities for the compression tests.

References

[1] Hunt MO, Suddarth SK. Prediction of elastic constants of particleboard. Forest Prod J 1974;24(5):52–7.

[2] Triche MH, Hunt MO. Modeling of parallel-aligned wood strand composites. Forest Prod J 1993;43(11/12):33–44.
[3] Cha JK, Pearson RG. Stress Analysis and prediction in 3-layer laminated veneer lumber: response to crack and grain angle. Wood and Fiber Sci 1994;26(1):97–106.
[4] Wang YT, Lam F. Computational modeling of material failure for parallel-aligned strand based wood composites. Computational Material Science 1998;11:157–65.
[5] Clouston P, Lam F. Computational modeling of strand-based wood composites. J Eng Mech 2001;127(8):844–51.
[6] Tsai SW, Wu EM. A general theory of strength for anisotropic materials. J Comp Mater 1971;5:58–80.
[7] Shih CF, Lee D. Further developments in anisotropic plasticity. Trans ASME, J Eng Mater Technol 1978;100:294–302.
[8] Owen DRJ, Hinton E. Finite elements in plasticity. New York: McGraw-Hill; 1980.
[9] Barrett JD, Foschi RO, Fox SP. Perpendicular-to-grain strength of Douglas-fir. Can J Civ Eng 1975;2(1):50–7.
[10] Madsen B, Buchanan AH. Size effects in timber explained by a modified weakest-link theory. Can J Civ Eng 1986;13(2):218–32.
[11] Barrett JD, Lam F, Lau W. Size effects in visually graded softwood structural lumber. J Mater Civ Eng 1995;7(1):19–30.
[12] Clouston P, Lam F, Barrett JD. Incorporating size effects in the Tsai–Wu strength theory for Douglas-fir laminated veneer. Wood Science and Technology 1998;32:215–26.
[13] Clouston, P. The Tsai–Wu strength theory for Douglas-fir laminated veneer. Master of Applied Science Thesis, University of British Columbia, Vancouver, B.C. Canada; 1995.
[14] Bodig J, Jayne BA. Mechanics of wood and wood composites. Malabar (FL): Krieger Publishing Co; 1993.
[15] Standard methods of testing static tests of timbers in structural sizes. Philadelphia (PA): ASTM. D198, 1999.
[16] Dai C, Steiner PR. Spatial structure of wood composites in relation to processing and performance characteristics. Part 1. Rationale for model development. Wood Science and Technology 1993;28(1):45–51.
[17] Ellis S, Dubois J, Avramidis S. Determination of parallam macroporosity by two optical techniques. Wood and Fiber Science 1994;26(1):1–77.
[18] Sugimori M, Lam F. Macro-void distribution analysis in strand-based wood composites using and X-ray computer tomography technique. J Wood Sci 1999;45(3):254–7.
[19] Lu C. Organization of wood elements in partially oriented flakeboard mats. PhD thesis, University of British Columbia-Vancouver, B.C. Canada; 1999.